Energy analysis of the resonant frequency shift pattern induced by non-uniform blockages in pressurized water pipes

T. C. Che[1]; **H. F. Duan**, M.ASCE[2]; **B. Pan**[3]; **P. J. Lee**[4]; **M. S. Ghidaoui**, M.ASCE[5]

[1] Ph.D. Candidate, Department of Civil and Environmental Engineering, The Hong Kong Polytechnic University, Hung Hom, Kowloon, Hong Kong SAR, PR China. E-mail: tong-chuan.che@connect.polyu.hk

[2] Assistant Professor, Department of Civil and Environmental Engineering, The Hong Kong Polytechnic University, Hung Hom, Kowloon, Hong Kong SAR, PR China (corresponding author). E-mail: hf.duan@polyu.edu.hk

[3] Ph.D. Student, Department of Civil and Environmental Engineering, The Hong Kong Polytechnic University, Hung Hom, Kowloon, Hong Kong SAR, PR China. E-mail: bin.pan@connect.polyu.hk

[4] Professor, Department of Civil and Natural Resources Engineering, The University of Canterbury, Private Bag 4800, Christchurch, New Zealand. E-mail: pedro.lee@canterbury.ac.nz

[5] Chair Professor, Department of Civil and Environmental Engineering, The Hong Kong University of Science and Technology, Kowloon, Hong Kong SAR, PR China. E-mail: ghidaoui@ust.hk

Abstract

Blockages in urban water supply systems are commonly formed from various complicated physical, chemical, and biological processes; thus, they usually constrict randomly and non-uniformly along their lengths. Although the transient-based method has been developed for blockage detection, the applications of this method are mainly limited to blockages of uniform constriction along their lengths (termed as uniform blockages). The influence of blockages with linearly varying diameters (termed as linear non-uniform blockages) on transient frequency responses was studied by the authors in a previous study. It was found that the resonant frequency shifts induced by linear non-uniform blockages have totally different patterns from that of uniform blockages. Specifically, the resonant frequency shifts induced by linear non-uniform blockages become less evident for higher harmonics. But the physical mechanism of this pattern is still unclear. This study intends to clarify this phenomenon from an energy perspective. For this purpose, the energy transmission coefficient of an unbounded pipeline containing various blockages is analytically derived, which is numerically validated by the method of characteristics. Afterwards, the influence of non-uniform blockage properties on the energy transmission is investigated systematically based on the validated result. The results indicate that the impedance of non-uniform blockages is frequency dependent, which becomes smaller for higher frequency waves. This means that non-uniform blockages have a less blocking effect on the propagation of higher frequency waves; thus, the resonant frequency shifts induced by non-uniform blockages become less evident.

Keywords: Energy transmission coefficient; non-uniform blockage; resonant frequency shift; transfer matrix; transient; water pipeline

Introduction

In urban water supply systems, partial and extended blockages are commonly formed from a variety of complicated sources (e.g., chemical corrosion, biofilm accumulation, and sediment deposition) and tend to grow over time, which brings a great challenge to drinking water security as well as water and energy savings (Duan et al., 2012; Stephens, 2008). In addition, these extended blockages may significantly change the maximum and minimum pressure heads during hydraulic transients (Brunone et al., 2008; Lee et al., 2013; Tuck et al., 2013), and the changed pressure heads may exceed the original transient design capacity; thus, potentially increase the failure rate of pipeline systems. For these reasons, detection techniques are urgently needed to diagnose these blockages in early stage so as to minimize the resultant problems and wastage. Currently, internal inspection of pipelines by closed-circuit television cameras is a commonly used approach for extended blockage detection. These cameras are physically inserted into target pipelines to conduct a real-time internal inspection of the pipe wall condition (Henry & Luxmoore, 1996). This technique is more suitable for simple and small-scale pipeline systems, such as pipeline systems in thermal power plants, since inspection by closed-circuit television cameras is a slow, tedious, and costly process. Besides, it often requires the target pipelines to be off-line, and the service interruption will cause inconvenience to water users. Therefore, it is vital to develop an efficient, affordable, and non-destructive method for extended blockage detection.

In the last few decades, the transient-based method has been used for the detection of various pipeline faults including leaks (Brunone & Ferrante, 2001; Colombo et al., 2009; Covas & Ramos, 2010; Duan et al., 2011; Gong et al., 2014; Kim, 2016, 2018; Lee et al., 2006; Liggett & Chen, 1994; Sattar & Chaudhry, 2008; X. Wang & Ghidaoui, 2018), discrete blockages (Kim, 2016; Lee et al.,

2008; Meniconi et al., 2011a; Sattar et al., 2008; X. J. Wang et al., 2005), side branches with dead ends (Duan & Lee, 2015; Kim, 2016; Meniconi et al., 2011b, 2011c), and pipe wall corrosion (Gong et al., 2015). The principle of this method is that a transient wave, with a propagation speed around 1 km/s in elastic water pipelines, is injected into the target pipeline at a localized accessible point (e.g., a fire hydrant). Any fault in the pipeline (e.g., a leak or blockage) imposes an additional reflected wave to the injected wave; thus, the measured pressure wave echoes theoretically contains physical information that is useful for pipeline fault and system integrity identification. In recent years, the successful theoretical and experimental extensions of the transient-based method to extended blockage detection provide an alternative to traditional closed-circuit television cameras. Specifically, Brunone et al. (2008) observed that extended blockages have a significantly different influence on the time domain pressure echoes from discrete blockages, thus the transient-based method used for discrete blockage detection may not be applicable to extended blockages. Duan et al. (2012) and Tuck et al. (2013) found that extended blockages induce frequency shifts on the resonant peaks of pipeline systems, based on which an optimization-based method was proposed for the inverse detection of extended blockages in pressurized pipelines (Duan et al., 2012; Duan et al., 2013). This frequency domain method was further coupled with a time domain method (Meniconi et al., 2011a; Meniconi et al., 2011b) by Meniconi et al. (2013) to further improve its computational accuracy and efficiency. Afterwards, Louati et al. (2018) explained the physical mechanism of the resonant frequency shifts induced by extended blockages using the Bragg resonance theory.

While the transient-based method has demonstrated its potential for extended blockage detection, this method is developed based on blockages of uniform constriction along their lengths (termed as uniform blockages), which is equivalent to multiple pipelines with different diameters connected in

84 series (Meniconi et al., 2012). Extended blockages in real urban water supply systems are usually
85 formed from various complicated physical, chemical, and biological processes; thus, as shown in Figs.
86 1(a) and 1(b), these blockages usually constrict randomly and non-uniformly along their lengths.
87 Inaccuracy and invalidity of the current transient-based method have been observed in laboratories for
88 non-uniform blockage detection (Duan et al., 2017). Therefore, understanding the interaction between
89 transient waves and non-uniform blockages is necessary to enhance the practical applications of the
90 transient-based method for extended blockage detection.

91 Recently, the authors studied the influence of linear non-uniform blockages, whose diameters
92 vary linearly along their lengths, on transient frequency responses (Che et al., 2018b). It was found
93 that linear non-uniform blockages give rise to significantly different resonant frequency shift patterns
94 from uniform blockages. Specifically, the resonant frequency shifts induced by linear non-uniform
95 blockages become less evident for higher harmonics, but the physical mechanism of this pattern from
96 analytical and numerical results is still unclear.

97 As a continuation of the previous study on linear non-uniform blockages (Che et al., 2018b), this
98 paper intends to: (1) investigate the resonant frequency shift pattern induced by other non-linear
99 non-uniform blockages, whose diameters vary exponentially along their lengths (termed as
100 exponential non-uniform blockages), to generalize further the conclusions drawn in the previous study
101 (Che et al., 2018b); and (2) qualitatively explain the physical mechanism of the non-uniform blockage
102 induced resonant frequency shift pattern from an energy perspective. To this end, the overall transfer
103 matrices of pipeline systems with exponential non-uniform blockages are derived to realize Aim (1).
104 To achieve Aim (2), the energy transmission coefficients of blocked pipeline systems are analytically
105 derived based on the system overall transfer matrices obtained in Aim (1). The results and findings of

106 this study are expected to provide scientific basis for method development of blockage detection in
107 urban water supply systems.

108 **Models and Methods**

109 ***Overall Transfer Matrix of a Pipeline System with Exponential Non-uniform Blockages***

110 To facilitate the analytical analysis, the real blockages in Fig. 1(b) are simplified into a series of
111 exponential non-uniform blockages, as shown in Fig. 1(c), whose radiuses change exponentially along
112 the axial direction. The one-dimensional (1D) wave equation in the frequency domain for the *n*-th
113 exponential non-uniform blockage in Fig. 1(c) is (Che et al., 2017; Che et al., 2018b)

114 $$\frac{d^2 p_n}{dx^2} + \frac{A_n'}{A_n}\frac{dp_n}{dx} + k_0^2 p_n = 0 \tag{1}$$

115 where p = pressure deviation from the mean in the frequency domain; x = distance along the pipeline;
116 $A = A(x)$ = pipe cross-sectional area; A' = derivative of A; $k_0 = \omega/a_0$ = wave number in intact pipe
117 sections, in which ω = angular frequency, a_0 = wave speed; subscript n = the n-th exponential
118 non-uniform blockage in Fig. 1(c).

119 Note that a frictionless pipeline system with an elastic pipe wall is firstly considered in the
120 analytical analysis to highlight the interaction between transient waves and non-uniform blockages
121 (Che et al., 2018b; Duan et al., 2014). The influence of friction on the derived analytical result will be
122 further discussed in the numerical validation. In addition, it was found by the authors in a previous
123 study (Che et al., 2018b) that the wave speed a_b within blockages has a limited influence on the
124 overall resonant frequency shift pattern induced by non-uniform blockages. Therefore, to simplify the
125 problem, the transient wave speed is assumed to be constant throughout the pipeline (i.e., $a(x) = a_0$).

126 As shown in Fig. 1(c), the pipe radius of the *n*-th exponential non-uniform blockage is defined as

127 $$r_n(x) = R_{Ln} e^{s_n x} \tag{2}$$

where r_n = pipe radius of the n-th exponential non-uniform blockage; R_{Ln} = pipe radius at the left boundary of the n-th exponential non-uniform blockage; s_n = a coefficient that determines the radius changing rate of the n-th exponential non-uniform blockage, which is defined as $s_n = \ln(R_{Rn}/R_{Ln})/l_n$, where R_{Rn} = pipe radius at the right boundary of the n-th exponential non-uniform blockage, l_n = length of the n-th exponential non-uniform blockage. Then, the cross-sectional area of the n-th exponential non-uniform blockage A_n and its derivative A_n' in Eq. (1) can be determined. Substituting A_n and A_n' into Eq. (1), the 1D wave equation for the n-th exponential non-uniform blockage becomes

$$\frac{d^2 p_n}{dx^2} + 2s_n \frac{dp_n}{dx} + k_0^2 p_n = 0 \tag{3}$$

Using the plane wave solution $p_n = e^{-ikx}$ as a trial solution of Eq. (3), results in the following dispersion relation

$$k^2 + 2is_n k - k_0^2 = 0 \tag{4}$$

where i = imaginary number; k = wave number. The solutions of Eq. (4) are (Che et al., 2017)

$$k = \pm\sqrt{k_0^2 - s_n^2} - is_n \tag{5}$$

Thus, the following general solutions for the n-th exponential non-uniform blockage can be obtained

$$p_n = \frac{C_1 e^{ik'x} + C_2 e^{-ik'x}}{R_{Ln} e^{s_n x}} \tag{6}$$

where $k' = (k_0^2 - s_n^2)^{1/2}$ = the group wave number of transient waves in the exponential non-uniform blockage; C_1 and C_2 are two constants.

The general solutions in Eq. (6) are a linear superposition of the incident and reflected waves propagating towards opposite directions. Moreover, in the case of exponential non-uniform blockages, $|s_n|$ represents the cutoff wave number. At wave numbers lower than $|s_n|$ (i.e., $k_0 < |s_n|$), k' is imaginary. The general solutions in Eq. (6) become evanescent waves, which decay along the pipeline and do not propagate as true transient pressure waves (Blackstock, 2000).

Based on the general solutions in Eq. (6), the transfer matrix of the n-th exponential non-uniform blockage in Eq. (7) connecting two state vectors at two boundaries is obtained (Che et al., 2017; Che et al., 2018b). Note that the pressure deviation p is transformed into the pressure head deviation h, which is a common practice in hydraulic engineering.

$$\begin{pmatrix} q \\ h \end{pmatrix}_{n+1} = \begin{pmatrix} U_{11} & U_{12} \\ U_{21} & U_{22} \end{pmatrix} \begin{pmatrix} q \\ h \end{pmatrix}_{n} \tag{7}$$

where subscripts n and n+1 are the upstream and downstream boundaries of the n-th exponential non-uniform blockage, respectively; q = discharge deviation in the frequency domain; h = pressure head deviation in the frequency domain; U_{ij} = transfer matrix elements, which are as follows:

$$U_{11} = \frac{S_{n+1}}{S_n} \frac{\left(ik' - s_n\right)e^{ik'l_n} + \left(ik' + s_n\right)e^{-ik'l_n}}{2ik'e^{s_n l_n}}$$

$$U_{12} = \frac{S_{n+1} g \left(ik' - s_n\right)\left(ik' + s_n\right)}{\omega} \frac{e^{ik'l_n} - e^{-ik'l_n}}{2k'e^{s_n l_n}}$$

$$U_{21} = \frac{\omega}{S_n g} \frac{-e^{ik'l_n} + e^{-ik'l_n}}{2k'e^{s_n l_n}}$$

$$U_{22} = \frac{\left(ik' + s_n\right)e^{ik'l_n} + \left(ik' - s_n\right)e^{-ik'l_n}}{2ik'e^{s_n l_n}}$$

where g = gravitational acceleration; S_n and S_{n+1} = pipe cross-sectional areas at the upstream and downstream boundaries of the n-th exponential non-uniform blockage, respectively.

Note that the uniform pipeline is one special case of the exponential non-uniform blockage. Let $s_n = 0$, which is equivalent to a single uniform pipeline, Eq. (7) becomes

$$\begin{pmatrix} q \\ h \end{pmatrix}_{n+1} = \begin{pmatrix} \cos\left(k_0 l_n\right) & -i\dfrac{S_{n+1} g}{a_0}\sin\left(k_0 l_n\right) \\ -i\dfrac{a_0}{S_n g}\sin\left(k_0 l_n\right) & \cos\left(k_0 l_n\right) \end{pmatrix} \begin{pmatrix} q \\ h \end{pmatrix}_{n} \tag{8}$$

which is consistent with previous studies on transfer matrices of uniform pipelines (Chaudhry, 2014; Wylie et al., 1993). The overall transfer matrix of a blocked pipeline system, as shown in Fig. 1(c),

can be produced by multiplying individual matrices of each pipe component in the order of their locations (Chaudhry, 2014; Duan et al., 2012; Lee et al., 2006; Wylie et al., 1993).

$$\begin{pmatrix} q \\ h \end{pmatrix}_1 = \begin{pmatrix} \cos(k_0 l_1) & -i\dfrac{S_2 g}{a_0}\sin(k_0 l_1) \\ -i\dfrac{a_0}{S_1 g}\sin(k_0 l_1) & \cos(k_0 l_1) \end{pmatrix} \times \cdots \times \begin{pmatrix} (U_{11})_n & (U_{12})_n \\ (U_{21})_n & (U_{22})_n \end{pmatrix} \times \cdots \times \begin{pmatrix} \cos(k_0 l_N) & -i\dfrac{S_{N+1} g}{a_0}\sin(k_0 l_N) \\ -i\dfrac{a_0}{S_N g}\sin(k_0 l_N) & \cos(k_0 l_N) \end{pmatrix} \begin{pmatrix} q \\ h \end{pmatrix}_{N+1} \tag{9}$$

where subscripts "1" and "N+1" are locations of upstream and downstream boundaries of a blocked pipeline system, as shown in Fig. 1(c), respectively. Rewrite Eq. (9) in the following simplified form

$$\begin{pmatrix} q \\ h \end{pmatrix}_1 = \begin{pmatrix} U_{11}^* & U_{12}^* \\ U_{21}^* & U_{22}^* \end{pmatrix} \begin{pmatrix} q \\ h \end{pmatrix}_{N+1} \tag{10}$$

where U_{ij}^* = elements of the system overall transfer matrix.

Energy Transmission Coefficient of an Unbounded Blocked Pipeline System

Based on the above overall transfer matrix in Eq. (10), the energy transmission coefficient of an unbounded blocked pipeline system is derived in this section. To simplify the problem, a pipeline system with two symmetrical exponential non-uniform blockages (i.e., $l_2 = l_3$), as shown in Fig. 2, is selected for investigation. Note that the derived energy transmission coefficient can be also applied to pipeline systems with multiple non-uniform blockages (see Fig. 1(c)) as long as the system overall transfer matrices are determined.

In physics, a transient wave is a pressure disturbance that travels through fluids, accompanied by a transfer of energy. The energy transmission coefficient of a blocked pipeline system with anechoic boundaries (i.e., located at A and E), as shown in Fig. 2, is defined as the ratio between the energy flow (i.e., power) transmitted through the non-uniform blockages (W_{tr}) and that incident on the

187 non-uniform blockages (W_{in}).

188 $$T_C = \frac{W_{tr}}{W_{in}} \tag{11}$$

189 where T_C = energy transmission coefficient.

190 By applying the above-defined energy transmission coefficient T_C in Eq. (11) to the classical
191 water hammer theory (note that the detailed derivation procedure is provided in Appendix), finally the
192 T_C can be represented by the overall transfer matrix elements U_{ij}^* in Eq. (10).

193 $$T_C = \left| \frac{2}{\frac{gS_0U_{21}^*}{a_0} + U_{22}^* + U_{11}^* + \frac{a_0U_{12}^*}{gS_0}} \right|^2 \tag{12}$$

194 where S_0 = cross-sectional areas at two boundaries A and E in Fig. 2.

195 **Energy Transmission Coefficient Pattern and Its Physical Mechanisms**

196 ***Energy Transmission Coefficient Patterns of Pipeline Systems with Various Blockages***

197 Based on the derived energy transmission coefficient T_C in Eq. (12), the T_C patterns of pipeline
198 systems with various blockages are visualized in this section. Because the following results involve
199 the Bragg's law, there is a need to review related fundamental theory herein. The Bragg's law was
200 firstly proposed by Bragg and Bragg (1913) in the process of investigating the composition of X-rays.
201 It relates the wavelength of the X-ray and the distance between crystal atomic sheets to the angles at
202 which an impinging X-ray beam would be reflected. Recently, the Bragg resonance phenomena of
203 transient waves in a pressurized water pipeline containing a single uniform blockage were studied by
204 Louati et al. (2018). As shown in Fig. 3(a), an incident wave with a certain wave length (λ) impinges
205 on the uniform blockage from the right end (i.e., Location E). From Location E to Location A, this
206 incident wave first encounters a sudden constriction at Junction D and then a sudden expansion at
207 Junction B. The incident wave is partially reflected at these junctions. According to the Joukowsky's

208 equation (Joukowsky, 1898), the sign of the reflected wave from Junction D keeps the same with the
209 incident wave. In contrast, the reflected wave from Junction B is opposite in sign to the incident wave.
210 In addition, the reflected wave from Junction B travels a distance $2(l_2 + l_3)$ more than the wave
211 reflected by Junction D. Because these two reflected waves from Junctions B and D are opposite in
212 sign, they experience destructive interference at Junction D when $j\lambda = 2(l_2 + l_3)$, where $j = 1, 2, 3\ldots$.
213 On this occasion, the incident wave has the maximum transmission. Conversely, these two reflected
214 waves experience constructive interference at Junction D when $(2j + 1)\lambda/2 = 2(l_2 + l_3)$, then the
215 incident wave has the minimum transmission.

216 Whereas the Bragg resonance condition of non-uniform blockages in this study is different from
217 that of uniform blockages investigated in the previous study of Louati et al. (2018). As shown in Figs.
218 3(b) and 3(c), from Location E to Location A, the incident wave first encounters a continuous
219 constriction between Junctions C and D and then a continuous expansion between Junctions B and C.
220 On average, the waves reflected by the continuous expansion only travel a distance $2l_3$ (note that $l_2 =$
221 l_3 in this study) more than the reflected waves from the continuous constriction. Therefore, these two
222 regional waves reflected by the continuous constriction and expansion have destructive interference
223 when $j\lambda = 2l_3$ and constructive interference when $(2j + 1)\lambda/2 = 2l_3$.

224 The derived energy transmission coefficients T_C in Eq. (12) of unbounded pipeline systems
225 containing uniform or non-uniform (including linear and exponential) blockages are visualized in Fig.
226 4. Note that these blockages have the same blocked volume. The T_C curve of an intact pipeline system
227 is also plotted in Fig. 4 for convenient comparison. The detailed parameters of these 4 cases are listed
228 in Table 1, in which R = radius of an intact pipe; R_C = pipe radius at Junction C in Fig. 3; $|s|$ = the
229 radius changing rate of non-uniform blockages; "exp" = is short for "exponential".

As shown in Fig. 4, the incident wave frequency is normalized by the minimum destructive interference frequency of the blockages, which is $2\pi(a_0/(2(l_2 + l_3)))$ for uniform blockages and $2\pi(a_0/(2l_3))$ for non-uniform blockages, and is expressed as ω^*. According to Fig. 4, the energy transmission coefficient T_C of the intact pipeline system keeps the constant value of 1, which is physically reasonable since the incident wave should be entirely transmitted through an intact pipeline without any reflection. However, the T_C curves of three blocked pipeline systems are highly frequency dependent. Specifically, the T_C curve of the uniform blocked pipeline system fluctuates periodically with constant extent. This is consistent with previous studies on uniform blockages (Duan et al., 2014; Louati et al., 2018). Although the T_C curves of these two pipeline systems with non-uniform blockages also fluctuate periodically, their extent gradually becomes less evident for higher frequency incident waves. This means that the higher the incident wave frequency, the more energy is transmitted through these two non-uniform blockages. Note that the maximum frequency of the incident wave should be below the cut-off frequency of the first radial mode (M1), otherwise the plane wave assumption imposed in this 1D study may be violated (Che et al., 2018a; Louati & Ghidaoui, 2017). The physical mechanisms that govern these T_C patterns in Fig. 4 will be further explained in the following section (note that the following discussion mainly focuses on exponential non-uniform blockages, and more detailed information about the energy analysis of linear non-uniform blockages can be found in the conference paper (Che et al., 2018c).

Physical Mechanisms of Energy Transmission Coefficient Patterns

Based on Eq. (19) in Appendix and the frictionless 1D water hammer model, the impedance of a blocked pipeline system can be written as

$$Z = \frac{p}{q} = \frac{Z_{sp}}{A} = \frac{\rho_0 \omega}{kA} \tag{13}$$

where Z = impedance; Z_{sp} = specific impedance; ρ_0 = fluid density. Substituting the forward propagating wave in Eq. (5) (i.e., keep the "+" sign) into Eq. (13), gives

$$Z_n = \frac{\rho_0 \omega}{A\left(\sqrt{k_0^2 - s_n^2} - i s_n\right)} = \frac{\rho_0 a_0}{A\left(\sqrt{1-\left(\frac{s_n}{k_0}\right)^2} - i\frac{s_n}{k_0}\right)} = \frac{\rho_0 a_0}{A}\left(\sqrt{1-\left(\frac{s_n}{k_0}\right)^2} + i\frac{s_n}{k_0}\right) = \frac{\rho_0 a_0}{A}\left(\sqrt{1-\left(\frac{\omega_{cut}}{\omega}\right)^2} + i\frac{\omega_{cut}}{\omega}\right) \quad (14)$$

where $\omega_{cut} = s_n a_0$ is the cutoff frequency of the n-th exponential non-uniform blockage.

Two physical mechanisms that govern the overall patterns of T_C in Fig. 4 are: (1) the Bragg's law; and (2) the impedance mismatch between the intact and blocked pipe sections.

(1) Specifically, the fluctuation of energy transmission coefficient T_C curves in Fig. 4 is due to the Bragg's law. Take the uniform blockage in Fig. 3(a) for instance, the reflected waves (from Junctions B and D) of the incident wave at most frequencies would not experience constructive interference at Junction D, because these reflected waves would be out of phase (i.e., phase shift ranges from 0 to π), cancelling part of the reflected energy out. However, when the incident wave frequency is an integral multiple of the minimum destructive interference frequency of the blockage (i.e., $\omega^* = 1, 2, 3, 4, 5$ in Fig. 4) the reflected waves (from Junctions B and D) would be completely out of phase (i.e., phase shift is π), cancelling each other out. In such situations, the incident wave has the maximum transmission. Therefore, the fluctuation period of T_C curves in Fig. 4 is one unit of the minimum destructive interference frequency of the blockages.

(2) The fluctuating extent of energy transmission coefficient T_C curves in Fig. 4 is governed by the impedance mismatch (ΔZ) at Junction D between the intact (e.g., Pipe 4 in Fig. 3) and blocked (e.g., Pipe 3 in Fig. 3) pipe sections. For the pipeline with uniform blockages in Fig 3(a), the impedance mismatch at Junction D is $\Delta Z = \rho_0 a_0 (1/A_3 - 1/A_4)$, which is constant for the incident

wave of various frequencies, therefore its T_C curve would fluctuate with constant extent. While for the pipeline system with exponential non-uniform blockages in Fig. 3(b), the impedance of the blocked pipe section (i.e., Eq. (14)) is frequency dependent. In particular, the impedance of exponential non-uniform blockages gradually decreases as the increase of the incident wave frequency. This means the higher the incident wave frequency, the smaller is the impedance mismatch at Junction D (i.e., ΔZ tends to 0). On this occasion, higher frequency incident waves would feel a less blocking effect from the exponential non-uniform blockages; thus, more energy is transmitted through the non-uniform blockages, and the fluctuation of the T_C curve becomes less evident.

Numerical Validation

Energy Transmission Coefficient of a Frictionless Unbounded System

To validate the derived analytical result in Eq. (12), the classical frictionless 1D water hammer model is solved by the method of characteristics (MOC) (Chaudhry, 2014; Wylie et al., 1993). As shown in Fig. 2, an unbounded pipeline system with two anechoic boundaries (i.e., upstream and downstream) is used for the numerical validation. The original intact pipeline is blocked by exponential non-uniform blockages. The detailed parameters of this pipeline system are listed in Table 2. In the numerical experiment, exponential non-uniform blockages are approximated by stepwise discretized grids. The 1,000-m-long pipe is divided into 10,000 small computational reaches (i.e., spatial grid size $\Delta x \sim 0.1$ m) to reduce the reflection caused by numerical errors. The incident wave generated at the downstream generator is given by the formula in Eq. (15) (i.e., a Gaussian-modulated sinusoidal pulse) (Louati et al., 2018), and the pressure trace is measured by the wave receiver located at the upstream end.

$$P_{in} = P_0 + P_0 \exp\left(-4\left(\frac{\omega_c}{\beta}\right)^2 \log(10)\left(t - \left(\frac{\beta}{\omega_c}\right)^2\right)\right)\sin\left(\omega_c\left(t - \frac{\beta}{\omega_c}\right)\right) \quad (15)$$

where P_{in} = the incident wave pressure at the generator; P_0 = the initial pressure in the pipeline; ω_c = the angular central frequency of the incident wave; β = a coefficient that determines the frequency bandwidth of the incident wave; t = time; $0 < t \leq \beta/\omega_c$.

Two features of the Gaussian-modulated sinusoidal pulse in Eq. (15) are that: (1) most of the energy is distributed at its central frequency ω_c; and (2) the frequency bandwidth of this pulse can be determined by appropriately adjusting the value of β.

The incident wave generated by the downstream generator and the transmitted wave measured by the upstream receiver are plotted in Fig. 5(a). The pressure P is normalized according to $(P - P_0)/P_0$ and plotted as P^*. Fig. 5(a) indicates that the amplitude of the transmitted wave is almost identical to that of the incident wave. To explain this phenomenon, these time domain signals in Fig. 5(a) are transformed into the frequency domain in Fig. 5(b). It turns out that the central frequency of the incident wave is $\omega_c^* = 1.0$, as shown in Fig. 7, at which the energy transmission coefficient T_C has a local maximum value 1.00. This means reflected waves from the non-uniform blockages experience destructive interference (i.e., condition of minimum reflection or maximum transmission). On this condition, all the energy carried by this incident wave should be transmitted through the non-uniform blockages.

As shown in Fig. 7, three more points on the energy transmission coefficient T_C curve (i.e., at $\omega_c^* = 0.5$, 1.5, and 2.5) are further validated and discussed in detail herein. In Figs. 6(a) and 6(b), the amplitude of the transmitted wave is significantly less than that of the incident wave because of the low T_C value at the central frequency of the incident wave $\omega_c^* = 0.5$ (at which point $T_C = 0.71$, this means only 71 percent of the energy carried by the incident wave is transmitted through the

316 non-uniform blockages). Although ω_c^* = 1.5 and 2.5 are two local minimum points on the T_C curve in
317 Fig. 7, compared with the ω_c^* = 0.5 case, the amplitude of these transmitted waves gradually increases
318 as the increase of the incident wave frequency. This is because the exponential non-uniform blockages
319 have a less blocking effect on the propagation of higher frequency waves. According to Eq. (27) in the
320 Appendix and the normalized amplitudes in Figs. 6(b), 6(d), and 6(f), the T_C values of these three
321 points are calculated as 0.71, 0.96, and 0.99, respectively, which agree well with the analytical T_C
322 values 0.71, 0.96, and 0.99 in Fig. 7.

323 In addition, more points on the energy transmission coefficient T_C curve are numerically obtained
324 and plotted in Fig. 7. It shows good agreement between the numerical and analytical results, which
325 confirms the validity of the derived result in Eq. (12) as well as the analytical method in this study.

326 ***Influence of a Frictional Bounded System on the Derived Energy Transmission Coefficient***

327 The analytical result derived in Eq. (12) is based on an unbounded pipeline system without any
328 friction. However, in real urban water supply systems, the pipeline systems are commonly bounded by
329 various of boundaries (e.g., reservoir and valve). In addition, the friction would change the amplitude
330 of a transient wave propagating along an intact pipeline section. Therefore, it is necessary to further
331 investigate the influences of system boundaries and friction on the analytical result in Eq. (12). As
332 shown in Fig. 8, a pipeline system with an upstream reservoir and a downstream valve is adopted.
333 Both steady and unsteady friction (Vardy & Brown, 1995) are considered in this bounded system.
334 Detailed system parameters of bounded and unbounded pipeline systems are listed in Table 3, where f
335 = friction factor.

336 First, as shown in Fig. 9, the transient frequency responses of the bounded pipeline system with
337 friction are numerically obtained based on the transfer matrix method (Che et al., 2018b). The energy

transmission coefficients T_C of the bounded pipeline system are estimated by (Kinsler et al., 1999)

$$T_C = 1 - \frac{\delta h_m^2}{h_{mi}^2} = 1 - \frac{\left(h_{mb} - h_{mi}\right)^2}{h_{mi}^2} \tag{16}$$

where δh_m = the blockage induced amplitude change for the m-th resonant peak; h_{mi} = amplitude of the m-th resonant peak for the intact pipeline system; h_{mb} = amplitude of the m-th resonant peak for the pipeline system with non-uniform blockages.

The energy transmission coefficient T_C curves of bounded (based on Eq. (16)) and unbounded (based on Eq. (12)) pipeline systems are plotted in Fig. 10. According to Fig. 10, the overall phase and fluctuation trend of these two curves for two systems show good agreement. This means that the overall pattern of T_C curve for the bounded pipeline system with friction is also governed by two physical mechanisms: (1) the Bragg's law; (2) the impedance mismatch between the intact and blocked pipe sections. In addition, Fig. 10 indicates that the analytical result in Eq. (12) may underestimate the amount of energy transmitted through non-uniform blockages in a frictional bounded pipeline system, especially for relative low frequency incident waves (e.g., $\omega^* < 1$). One reason for this is that the energy transmission coefficient of the frictional bounded system is calculated based on the amplitude of resonant peaks, as shown in Eq. (16), which could be further reinforced by system boundaries.

Further Application and Result Analysis

Energy Explanation of the Non-uniform Blockage Induced Resonant Frequency Shift Pattern

Based on the validated analytical result in Eq. (12), the influences of non-uniform blockage properties (i.e., length and severity) on the energy transmission coefficient T_C of unbounded pipeline systems are systematically investigated in this section. Detailed system parameters can refer to Table 4. At the same time, to explain the non-uniform blockage induced resonant frequency shift patterns from an

energy perspective, the transient frequency responses of bounded pipeline systems (like Fig. 9), with the same system parameters (i.e., Table 4) as the unbounded systems, are also obtained.

First, the influence of non-uniform blockage severity on the energy transmission coefficient T_C of unbounded pipeline systems is studied. According to Table 4, the blockage lengths (i.e., l_2 and l_3) of Tests T1, T2, and T3 are fixed. From Test T1 to T3, the minimum radius R_C of the blockage gradually increase from 0.15 m to 0.20 m, which means the blockage becomes less severe. The T_C curves of these three tests are plotted in Fig. 11(a). It shows that the overall trend of these three curves is the same except for the T_C values at a specific frequency. Specifically, for a fixed incident wave frequency, more energy is transmitted through the non-uniform blockages as the blockages become less severe. This is obvious since less severe blockages should have a less blocking effect on the propagation of transient waves.

The resonant frequency shift patterns of bounded pipeline systems, with the same system parameters as Tests T1, T2, and T3, adapted from a previous study of the authors (Che et al., 2018b) are plotted in Fig. 11(b). The normalized resonant frequency shift of the m-th resonant peak is defined as $\delta\omega_m^* = \omega_{mb}^* - \omega_{mi}^*$ (like Fig. 9), where ω_{mi}^* = the m-th normalized resonance frequency of the intact pipeline system; ω_{mb}^* = the m-th normalized resonance frequency of the pipeline system with non-uniform blockages. As shown in Fig. 11(b), the fluctuation of resonant frequency shift patterns induced by non-uniform blockages becomes less evident as the incident wave frequency increases. A reasonable explanation for this is that non-uniform blockages, as shown in Fig. 11(a), have a less blocking effect on the propagation of higher frequency waves, thus the resonant frequency shifts in Fig. 11(b) induced by non-uniform blockages become less evident.

The influence of non-uniform blockage length on the energy transmission coefficient T_C of

unbounded pipeline systems is also investigated. As shown in Table 4, the minimum radius R_C (i.e., severity) of the blockages in Tests T1, T4, and T5 is fixed. The length of the non-uniform blockages gradually decreases from 100 m to 1 m. As shown in Figs. 12(a) and 12(b), the obtained T_C curves (for unbounded system) and resonant frequency shift patterns (for bounded system) are similar with previous tests. Moreover, both T_C curves and resonant frequency shift patterns of these three tests almost coincide with each other. This means that the non-uniform blockage length has a limited influence on the amount of energy transmitted through non-uniform blockages. Thus, these three tests with various blockage lengths have the same blocking effect on the propagation of transient waves.

Preliminary Applications to Interpreting Laboratory Data

As shown in Fig. 13, two types of irregular blockages, made of aggregate or coir, have been investigated in the laboratory by the authors for their influences on transient wave behavior (Duan et al., 2017). But the influence of exponential non-uniform blockages has not yet well verified due to the difficulty of constructing perfectly exponential non-uniform blockages in laboratories. Therefore, as a preliminary application, the irregular blockage made of coir (with a mean roughness height of 3 mm) used in Duan et al. (2017) is selected and approximated by uniform and exponential non-uniform blockages (see Fig. 13). Then, the validity of two blockage approximation methods for transmission coefficient estimations is studied and discussed. Note that these two approximated uniform and non-uniform blockages have the same blocked volume. The experiment system consists of an upstream reservoir, a pipeline with irregular blockages (like A to E in Fig. 8), and a downstream discharge tank. Detailed system parameters are listed in Table 5, where l_b, $\bar{R}_b$, and $\bar{a}_b$ are the length, average radius, and average wave speed of the blocked section, respectively. More detailed experimental settings and operations are reported in Duan et al. (2017).

Because the experimental data in the frequency domain become relatively noisy for higher harmonics, only the first ten peaks are selected to calculate the energy transmission coefficient T_C based on Eq. (16). The T_C curves of the bounded pipeline system with irregular blockages (Eq. (16)) as well as corresponding unbounded pipeline systems with two approximated blockages (Eq. (12)) are plotted in Fig. 14. As shown in Fig. 14(a), when the irregular blockage is simplified into a uniform blockage, the periods (i.e., 1.00 and 1.16) of two T_C curves agrees well, but the energy transmission estimation is quite inaccurate. In contrast, according to Fig. 14(b), the approximation in exponential non-uniform blockages has a relatively good estimation of energy transmission, but the period agreement is relatively poor (i.e., 0.58 and 1.00). This can be attributed to the simplicity of current approximations, and detailed physical mechanisms of the interaction between transient waves and irregular blockages cannot be wholly represented by these two simplified blockages.

Implications and Recommendations

In previous studies (Duan et al., 2014; Louati et al., 2018), the amplitude (equivalent to energy) of transmitted and reflected waves of a uniform blockage in an unbounded pipeline system, as shown in Fig. 3(a), was obtained by applying the mass and momentum conservation at pipe junctions (i.e., Junctions B and D in Fig. 3(a)). However, the cross area of a pipeline system with non-uniform blockages, as shown in Figs. 3(b) and 3(c), changes continuously along its axial direction. This means that the cross areas of intact and blocked pipe sections are the same at pipe junctions. Therefore, the previous method (Duan et al., 2014; Louati et al., 2018) cannot be used for calculating the energy transmission coefficients T_C of a pipeline system containing non-uniform blockages. Based on the overall transfer matrix in Eq. (10), this paper proposes a new approach that is suitable for calculating the energy transmitted through non-uniform blockages in an unbounded pipeline system. In addition,

426 the derived result in Eq. (12) can be also applied to unbounded pipeline systems with multiple
427 blockages, which are more practical, once the system overall transfer matrices are determined.

428 The results and findings above demonstrate that two physical mechanisms govern the overall
429 pattern of energy transmission coefficient T_C in Fig. 4: (1) the Bragg's law; and (2) the impedance
430 mismatch between intact and blocked pipe sections. The fluctuation of these T_C curves is due to the
431 Bragg's law, and the fluctuation extent is determined by the impedance mismatch between intact and
432 blocked pipe sections. The impedance of exponential non-uniform blockages is frequency dependent,
433 which becomes smaller for higher frequency waves. This means that the higher the incident wave
434 frequency, the smaller the impedance mismatch between intact and blocked pipe sections. On this
435 occasion, higher frequency waves would feel a less blocking effect from exponential non-uniform
436 blockages. Therefore, more energy of higher frequency waves is transmitted through the non-uniform
437 blockages, and the induced resonant frequency shifts become less evident.

438 In practical applications of non-uniform blockage detection, it is a preferable and labour-saving
439 way to place the transient wave receiver at the same accessible point with the generator.
440 Understanding the energy transmission coefficient T_C curve of incident waves with various
441 frequencies provide valuable insights into the blocking effect of non-uniform blockages on transient
442 waves. It is useful for the selection of incident wave frequency and bandwidth to ensure that the
443 reflected waves contain enough energy for the pressure transducer (i.e., receiver) to measure.
444 Otherwise, the reflected waves, which have limited energy, may be buried by the background noises.
445 In this case, the useful resonant frequency shifts of this measured signal may be less evident that
446 cannot be used to detect non-uniform blockages accurately.

The preliminary application of the derived result in the laboratory indicates that approximations of the irregular blockage into a single uniform or exponential non-uniform blockage only have a reasonable estimation in either the phase or the amplitude of the real energy transmission coefficients. This is due to the relatively simple geometry of two approximated blockages, which is unable to capture the complex interaction between transient waves and irregular blockages. Therefore, it is necessary to further investigate the transient wave behaviour in a series of jointed non-uniform blockages (i.e., irregular blockage) and its influence on energy transmission coefficients. In this regard, the derived transmission coefficient in Eq. (12) is also applicable to an appropriate combination of multiple and different non-uniform blockages, which may form as a more realistic irregular blockage (like Fig. 1(c)), once the overall transfer matrix of this combination is determined.

Conclusions

This paper explains the resonant frequency shift pattern induced by non-uniform blockages in pressurised water pipelines from an energy perspective. First, the overall transfer matrix of a pipeline system containing exponential non-uniform blockages is analytically derived based on the 1D plane wave solutions. The overall transfer matrix is then used to derive the energy transmission coefficient of the unbounded pipeline system, which is numerically validated by the method of characteristics. Finally, the resonant frequency shift pattern of bounded pipeline systems with non-uniform blockages is explained by energy transmission curves of unbounded pipeline systems.

The results indicate that the exponential non-uniform blockages have a less blocking effect on the propagation of higher frequency waves. This is because the impedance of non-uniform blockages is frequency dependent, which becomes smaller for higher frequency waves. Therefore, the non-uniform blockage induced resonant frequency shifts become less evident for higher harmonics. In

practical applications of non-uniform blockage detection, the frequency and bandwidth of the incident wave should be selected carefully according to the energy transmission coefficient T_C curve to ensure that the reflected wave contains enough energy for pressure transducers to measure.

The preliminary applications to interpreting laboratory data indicates that further experimental and numerical verification of the derived result, as well as further investigation on the influence of irregular blockages on transient wave behaviour are needed in the future work.

Appendix

Detailed Derivation Procedure of the Energy Transmission Coefficient

As shown in Fig. 2, at the upstream and downstream boundaries of the pipeline system (i.e., locations A and E), the energy flow (i.e., power) passing through a unit cross-sectional area (termed as power intensity) is defined as (Blackstock, 2000)

$$I = \frac{1}{T}\int_0^T p^* u^* dt \tag{17}$$

where I = power intensity; $T = 2\pi/\omega$ for time-harmonic waves; p^* = pressure deviation from the mean in the time domain; u^* = axial velocity deviation from the mean in the time domain; t = time.

In classical acoustics, including water hammer problems focused on herein, it is often assumed that p^* and u^* are time-harmonic waves (Chaudhry, 2014; Che et al., 2018b)

$$p^* = pe^{i\omega t}, \quad u^* = ue^{i\omega t} \tag{18}$$

where p and u are complex amplitude. Specifically, let $u = |u|e^{i\theta}$, where $|u|$ = amplitude; θ = phase.

In the transient pipe flow analysis, the specific impedance is usually used for describing the transient wave propagation characteristics in specified pipelines, which is defined as

$$Z_{\mathrm{sp}} = \frac{p^*}{u^*} = \frac{p}{u} = \mathrm{Re}\left(Z_{\mathrm{sp}}\right) + i\,\mathrm{Im}\left(Z_{\mathrm{sp}}\right) = \left|Z_{\mathrm{sp}}\right| e^{i\phi} \tag{19}$$

where Z_{sp} = specific impedance; "Re" = real part; "Im" = imaginary part; Re(Z_{sp}) = resistance; Im(Z_{sp})

491 = reactance; ϕ = phase angle between p^* and u^*. Substituting Eq. (19) into Eq. (17), it becomes

$$\begin{aligned} I &= \frac{\omega}{2\pi}\int_0^{2\pi/\omega} \mathrm{Re}\left(Z_{\mathrm{sp}}u^*\right)\mathrm{Re}\left(u^*\right)dt \\ &= \frac{\omega}{2\pi}\int_0^{2\pi/\omega} \left|Z_{\mathrm{sp}}\right|\left|u\right|^2 \cos\left(\omega t+\theta+\phi\right)\cos\left(\omega t+\theta\right)dt \\ &= \frac{1}{2}\left|u\right|^2\left|Z_{\mathrm{sp}}\right|\cos\phi \\ &= \frac{1}{2}\left|u\right|^2\mathrm{Re}\left(Z_{\mathrm{sp}}\right) \end{aligned} \tag{20}$$

493 As shown in Fig. 2, for the upstream (i.e., location A) and downstream (i.e., location E) boundaries
494 with a cross-sectional area S_0, the energy flow passing through this area is

$$W = IS_0 = \frac{1}{2}\left|u\right|^2\mathrm{Re}\left(Z_{\mathrm{sp}}\right)S_0 \tag{21}$$

496 where W = energy flow; S_0 = the pipe cross-sectional area of intact junctions.

497 The energy transmission coefficient T_C of a blocked pipeline system with anechoic boundaries
498 (i.e., located at A and E), as shown in Fig. 2, is defined as the ratio between the energy flow
499 transmitted through the non-uniform blockage (W_{tr}) and that incident on the blockage (W_{in}).

$$T_C = \frac{W_{tr}}{W_{in}} \tag{22}$$

501 The general solutions of p for the 1D wave equation in intact Pipe 1 and Pipe 4, as shown in Fig. 2,
502 are (Duan et al., 2014)

$$p = Me^{-ik_0x} + Ne^{ik_0x} \tag{23}$$

504 where M and N are amplitude of the incident and reflected waves, respectively.

505 Substituting Eq. (23) into the frictionless 1D water hammer model, the following general
506 solutions of u can be obtained

$$u = \frac{1}{\rho_0 a_0}\left(Me^{-ik_0x} - Ne^{ik_0x}\right) \tag{24}$$

508 where ρ_0 = fluid density. The energy flow generated at the downstream boundary (i.e., located at E) is

$$W_{in} = \frac{1}{2\rho_0 a_0}\left|M_{\mathrm{E}}\right|^2\mathrm{Re}\left(Z_{\mathrm{sp}}\right)S_0 = \frac{\left|M_{\mathrm{E}}\right|^2}{2}S_0 \tag{25}$$

where M_E = amplitude of the incident wave generated at the downstream boundary (i.e., located at E).

Similarly, the energy flow transmitted through the non-uniform blockages (i.e., measured at A) is

$$W_{tr} = \frac{1}{2\rho_0 a_0}\left|M_A\right|^2 \mathrm{Re}\left(Z_{sp}\right) S_0 = \frac{\left|M_A\right|^2}{2} S_0 \tag{26}$$

where M_A = amplitude of the transmitted wave recieved at the upstream boundary (i.e., located at A).

Therefore, the energy transmission coefficient T_C of the unbounded blocked system in Fig. 2 is

$$T_C = \frac{W_{tr}}{W_{in}} = \left|\frac{M_A}{M_E}\right|^2 \tag{27}$$

The amplitude of a progressive wave keeps constant as it travels along a uniform pipe section (Munjal, 2014). Therefore, as shown in Fig. 2, M_A and M_E can be measured at any point along Pipe 1 and Pipe 4, respectively. To simplify the calculation, pipe lengths l_1 and l_4 can be taken as zero if necessary.

The overall transfer matrix (in terms of u and p) of a blocked pipeline system, as shown in Fig. 2, is

$$\begin{Bmatrix} u \\ p \end{Bmatrix}_D = \begin{bmatrix} V_{11}^* & V_{12}^* \\ V_{21}^* & V_{22}^* \end{bmatrix} \begin{Bmatrix} u \\ p \end{Bmatrix}_A \tag{28}$$

where V_{ij}^* = elements of the overall transfer matrix (in terms of u and p).

Based on the general solutions in Eqs. (23) and (24), the p and u at two locations A and D can be expressed as (note that $N_A = 0$)

$$p_A = M_A + N_A = M_A \tag{29a}$$

$$u_A = \frac{1}{\rho_0 a_0}\left(M_A - N_A\right) = \frac{M_A}{\rho_0 a_0} \tag{29b}$$

$$p_D = M_E + N_E \tag{29c}$$

$$u_D = \frac{1}{\rho_0 a_0}\left(M_E - N_E\right) \tag{29d}$$

From Eqs. (29a) to (29d)

$$M_{\mathrm{E}}=\frac{p_{\mathrm{D}}+\rho_0 a_0 u_{\mathrm{D}}}{2}=\frac{\left(V_{21}^{*}u_{\mathrm{A}}+V_{22}^{*}p_{\mathrm{A}}\right)+\rho_0 a_0\left(V_{11}^{*}u_{\mathrm{A}}+V_{12}^{*}p_{\mathrm{A}}\right)}{2}$$
$$=\frac{\left(V_{21}^{*}\dfrac{M_{\mathrm{A}}}{\rho_0 a_0}+V_{22}^{*}M_{\mathrm{A}}\right)+\rho_0 a_0\left(V_{11}^{*}\dfrac{M_{\mathrm{A}}}{\rho_0 a_0}+V_{12}^{*}M_{\mathrm{A}}\right)}{2} \tag{30}$$

The ratio between M_{A} and M_{E} is

$$\frac{M_{\mathrm{A}}}{M_{\mathrm{E}}}=\frac{2}{\dfrac{V_{21}^{*}}{\rho_0 a_0}+V_{22}^{*}+V_{11}^{*}+\rho_0 a_0 V_{12}^{*}} \tag{31}$$

Therefore, the energy transmission coefficient T_C can be represented by the overall transfer matrix elements V_{ij}^{*} (in terms of u and p)

$$T_C=\left|\frac{M_{\mathrm{A}}}{M_{\mathrm{E}}}\right|^2=\left|\frac{2}{\dfrac{V_{21}^{*}}{\rho_0 a_0}+V_{22}^{*}+V_{11}^{*}+\rho_0 a_0 V_{12}^{*}}\right|^2 \tag{32}$$

In terms of discharge q and pressure head h, the overall transfer matrix of the unbounded pipeline system in Fig. 2 is

$$\begin{Bmatrix} q \\ h \end{Bmatrix}_{\mathrm{D}}=\begin{bmatrix} U_{11}^{*} & U_{12}^{*} \\ U_{21}^{*} & U_{22}^{*} \end{bmatrix}\begin{Bmatrix} q \\ h \end{Bmatrix}_{\mathrm{A}} \tag{33}$$

Writing Eq. (33) in the equation form

$$S_{\mathrm{D}}u_{\mathrm{D}}=U_{11}^{*}S_{\mathrm{A}}u_{\mathrm{A}}+U_{12}^{*}\frac{p_{\mathrm{A}}}{\rho_0 g} \tag{34a}$$

$$\frac{p_{\mathrm{D}}}{\rho_0 g}=U_{21}^{*}S_{\mathrm{A}}u_{\mathrm{A}}+U_{22}^{*}\frac{p_{\mathrm{A}}}{\rho_0 g} \tag{34b}$$

where S_{A} and S_{D} are the pipe cross-sectional areas at two boundaries A and D in Fig. 2, respectively.

Rewrite Eqs. (34) as

$$u_{\mathrm{D}}=\underbrace{\frac{S_{\mathrm{A}}}{S_{\mathrm{D}}}U_{11}^{*}}_{V_{11}^{*}}u_{\mathrm{A}}+\underbrace{\frac{U_{12}^{*}}{\rho_0 g S_{\mathrm{D}}}}_{V_{12}^{*}}p_{\mathrm{A}} \tag{35a}$$

$$p_{\mathrm{D}}=\underbrace{\rho_0 g S_{\mathrm{A}}U_{21}^{*}}_{V_{21}^{*}}u_{\mathrm{A}}+\underbrace{U_{22}^{*}}_{V_{22}^{*}}p_{\mathrm{A}} \tag{35b}$$

in which $S_{\mathrm{A}}=S_{\mathrm{D}}=S_0$. Therefore, the energy transmission coefficient T_C can be represented by overall

547 transfer matrix elements U_{ij}^{*} (in terms of q and h)

548
$$T_C = \left| \frac{2}{\frac{gS_0U_{21}^{*}}{a_0} + U_{22}^{*} + U_{11}^{*} + \frac{a_0U_{12}^{*}}{gS_0}} \right|^2 \tag{36}$$

549 **Acknowledgements**

550 This research work was supported by the research grants from: (1) the Hong Kong Research Grants
551 Council (projects no. T21-602/15-R, no. 25200616 and no. 15201017); and (2) the Hong Kong
552 Polytechnic University (projects no. 1-ZVCD and no. 1-ZVGF).

553 **Notations**

554 $A = A(x)$ = pipe cross-sectional area (m^2);

555 a_0 = wave speed (m/s);

556 "exp" = is short for "exponential";

557 g = gravitational acceleration (m/s^2);

558 h = pressure head deviation in the frequency domain (m);

559 I = power intensity (kg/s^3);

560 "Im" = imaginary part;

561 i = imaginary number;

562 k = wave number;

563 k_0 = wave number in intact pipe sections;

564 k' = group wave number in the exponential non-uniform blockage;

565 l_n = length of the n-th non-uniform blockage (or pipe) (m);

566 M, N = constants;

567 P = pressure in the time domain (Pa);

568 P^* = dimensionless pressure in the time domain;

569 P_{in} = the incident wave pressure at the generator (Pa);

570 P_0 = the initial pressure in the pipeline (Pa);

571 p^* = pressure deviation from the mean in the time domain (Pa);

572 p = pressure deviation from the mean in the frequency domain (Pa);

573 q = discharge deviation in the frequency domain (m^3/s);

574 R = radius of an intact pipe (m);

575 "Re" = real part;

576 R_C = pipe radius at Junction C (m);

577 $r = r(x)$ = pipe radius (m);

578 S_0 = pipe cross-sectional area of intact junctions (m^2);

579 S_n = pipe cross-sectional area at Junction n (m^2);

580 s = a coefficient that determines the radius changing rate of non-uniform blockages;

581 T_C = energy transmission coefficient;

582 t = time (s);

583 U_{ij} = transfer matrix elements;

584 U_{ij}^* = system overall transfer matrix elements;

585 V_{ij}^* = system overall transfer matrix elements (in terms of u and p);

586 u^* = axial velocity deviation from the mean in the time domain (m/s);

587 u = axial velocity deviation from the mean in the frequency domain (m/s);

588 W = energy flow ($kg \cdot m^2/s^3$);

589 x = distance along the pipeline (m);

590 Z = impedance (Pa·s/m^3);

591 $\delta\omega^*$ = normalized resonant frequency shift induced by blockages;

592 ρ_0 = fluid density (kg/m^3);

593 ω = angular frequency (rad/s);

594 ω^* = dimensionless angular frequency;

595 ω_c = angular central frequency of the incident wave (rad/s);

596 ω_{cut} = cutoff frequency of the exponential non-uniform blockage (rad/s).

597 **References**

598 Blackstock, D. T. (2000). *Fundamentals of physical acoustics*: John Wiley & Sons.

599 Bragg, W. H., & Bragg, W. L. (1913). The reflection of X-rays by crystals. *Proc. R. Soc. Lond. A,*
600 *88*(605), 428-438. doi:10.1098/rspa.1913.0040

601 Brunone, B., & Ferrante, M. (2001). Detecting leaks in pressurised pipes by means of transients.
602 *Journal of Hydraulic Research, 39*(5), 539-547. doi:10.1080/00221686.2001.9628278

603 Brunone, B., Ferrante, M., & Meniconi, S. (2008). Discussion of "detection of partial blockage in
604 single pipelines" by PK Mohapatra, MH Chaudhry, AA Kassem, and J. Moloo. *Journal of*
605 *Hydraulic Engineering, 134*(6), 872-874. doi:10.1061/(ASCE)0733-9429(2008)134:6(872)

606 Chaudhry, M. H. (2014). *Applied hydraulic transients*. New York: Springer-Verlag.

607 Che, T. C., Duan, H. F., Lee, P. J., & Ghidaoui, M. S. (2017). Theoretical analysis of the influence of
608 blockage irregularities on transient waves in water supply pipelines. *Paper presented at the*
609 *37th IAHR World Congress*, Kuala Lumpur, Malaysia.

610 Che, T. C., Duan, H. F., Lee, P. J., Meniconi, S., Pan, B., & Brunone, B. (2018a). Radial pressure
611 wave behavior in transient laminar pipe flows under different flow perturbations. *Journal of*
612 *Fluids Engineering, 140*(10), 101203. doi:10.1115/1.4039711

613 Che, T. C., Duan, H. F., Lee, P. J., Pan, B., & Ghidaoui, M. S. (2018b). Transient frequency responses
614 for pressurized water pipelines containing blockages with linearly varying diameters. *Journal*
615 *of Hydraulic Engineering, 144*(8), 04018054. doi:10.1061/(ASCE)HY.1943-7900.0001499

616 Che, T. C., Duan, H. F., Zheng, F., Pan, B., & Lee, P. J. (2018c). Energy analysis of transient

617 frequency shift pattern induced by non-uniform blockages in water pipelines. *Paper presented*
618 *at the 1st International WDSA/CCWI Joint Conference*, Kingston, Ontario, Canada.
619 Colombo, A. F., Lee, P. J., & Karney, B. W. (2009). A selective literature review of transient-based
620 leak detection methods. *Journal of Hydro-environment Research, 2*(4), 212-227.
621 doi:10.1016/j.jher.2009.02.003
622 Covas, D., & Ramos, H. (2010). Case studies of leak detection and location in water pipe systems by
623 inverse transient analysis. *Journal of Water Resources Planning and Management, 136*(2),
624 248-257. doi:10.1061/(ASCE)0733-9496(2010)136:2(248)
625 Duan, H. F., & Lee, P. J. (2015). Transient-based frequency domain method for dead-end side branch
626 detection in reservoir pipeline-valve systems. *Journal of Hydraulic Engineering, 142*(2),
627 04015042. doi:10.1061/(ASCE)HY.1943-7900.0001070
628 Duan, H. F., Lee, P. J., Che, T. C., Ghidaoui, M. S., Karney, B. W., & Kolyshkin, A. A. (2017). The
629 influence of non-uniform blockages on transient wave behavior and blockage detection in
630 pressurized water pipelines. *Journal of Hydro-environment Research, 17*, 1-7.
631 doi:10.1016/j.jher.2017.08.002
632 Duan, H. F., Lee, P. J., Ghidaoui, M. S., & Tuck, J. (2014). Transient wave-blockage interaction and
633 extended blockage detection in elastic water pipelines. *Journal of Fluids and Structures,*
634 *46*(2014), 2-16. doi:10.1016/j.jfluidstructs.2013.12.002
635 Duan, H. F., Lee, P. J., Ghidaoui, M. S., & Tung, Y. K. (2011). Leak detection in complex series
636 pipelines by using the system frequency response method. *Journal of Hydraulic Research,*
637 *49*(2), 213-221. doi:10.1080/00221686.2011.553486
638 Duan, H. F., Lee, P. J., Ghidaoui, M. S., & Tung, Y. K. (2012). Extended blockage detection in
639 pipelines by using the system frequency response analysis. *Journal of Water Resources*
640 *Planning and Management, 138*(1), 55-62. doi:10.1061/(ASCE)WR.1943-5452.0000145
641 Duan, H. F., Lee, P. J., Kashima, A., Lu, J., Ghidaoui, M. S., & Tung, Y. K. (2013). Extended blockage
642 detection in pipes using the system frequency response: analytical analysis and experimental
643 verification. *Journal of Hydraulic Engineering, 139*(7), 763-771.
644 doi:10.1061/(ASCE)HY.1943-7900.0000736
645 Gong, J., Stephens, M. L., Arbon, N. S., Zecchin, A. C., Lambert, M. F., & Simpson, A. R. (2015).
646 On-site non-invasive condition assessment for cement mortar–lined metallic pipelines by

time-domain fluid transient analysis. *Structural Health Monitoring, 14*(5), 426-438. doi:10.1177/1475921715591875

Gong, J., Zecchin, A. C., Simpson, A. R., & Lambert, M. F. (2014). Frequency response diagram for pipeline leak detection: comparing the odd and even harmonics. *Journal of Water Resources Planning and Management, 140*(1), 65-74. doi:10.1061/(ASCE)WR.1943-5452.0000298

Henry, R., & Luxmoore, A. R. (1996). A pipe-profiling adapter for CCTV inspection cameras: Development of a pipe-profiling instrument. *Measurement Science and Technology, 7*(4), 495-504. doi:10.1088/0957-0233/7/4/005

Joukowsky, N. E. (1898). Memoirs of the Imperial Academy Society of St. Petersburg. *Proceedings of the American Water Works Association, 24*, 341-424.

Kim, S. (2016). Impedance method for abnormality detection of a branched pipeline system. *Water Resources Management, 30*(3), 1101-1115. doi:10.1007/s11269-015-1213-6

Kim, S. (2018). Development of multiple leakage detection method for a reservoir pipeline valve system. *Water Resources Management, 32*(6), 2099-2112. doi:10.1007/s11269-018-1920-x

Kinsler, L. E., Frey, A. R., Coppens, A. B., & Sanders, J. V. (1999). *Fundamentals of acoustics*. New York: John Wiley & Sons.

Lee, P. J., Duan, H. F., Ghidaoui, M. S., & Karney, B. W. (2013). Frequency domain analysis of pipe fluid transient behaviour. *Journal of Hydraulic Research, 51*(6), 609-622. doi:10.1080/00221686.2013.814597

Lee, P. J., Lambert, M. F., Simpson, A. R., Vítkovský, J. P., & Liggett, J. A. (2006). Experimental verification of the frequency response method for pipeline leak detection. *Journal of Hydraulic Research, 44*(5), 693-707. doi:10.1080/00221686.2006.9521718

Lee, P. J., Vitkovsky, J. P., Lambert, M. F., Simpson, A. R., & Liggett, J. A. (2008). Discrete blockage detection in pipelines using the frequency response diagram: Numerical study. *Journal of Hydraulic Engineering, 134*(5), 658-663. doi:10.1061/(ASCE)0733-9429(2008)134:5(658)

Liggett, J. A., & Chen, L. C. (1994). Inverse transient analysis in pipe networks. *Journal of Hydraulic Engineering, 120*(8), 934-955. doi:10.1061/(ASCE)0733-9429(1994)120:8(934)

Louati, M., & Ghidaoui, M. S. (2017). High-frequency acoustic wave properties in a water-filled pipe. Part 1: dispersion and multi-path behaviour. *Journal of Hydraulic Research, 55*(5), 613–631. doi:10.1080/00221686.2017.1354931

677 Louati, M., Ghidaoui, M. S., Meniconi, S., & Brunone, B. (2018). Bragg-type resonance in blocked
678 pipe system and its effect on the eigenfrequency shift. *Journal of Hydraulic Engineering, 144*(1), 04017056. doi:10.1061/(ASCE)HY.1943-7900.0001383
679
680 Meniconi, S., Brunone, B., & Ferrante, M. (2011a). In-line pipe device checking by short-period
681 analysis of transient tests. *Journal of Hydraulic Engineering, 137*(7), 713-722.
682 doi:10.1061/(ASCE)HY.1943-7900.0000309
683 Meniconi, S., Brunone, B., & Ferrante, M. (2012). Water-hammer pressure waves interaction at
684 cross-section changes in series in viscoelastic pipes. *Journal of Fluids and Structures, 33*,
685 44-58. doi:10.1016/j.jfluidstructs.2012.05.007
686 Meniconi, S., Brunone, B., Ferrante, M., & Massari, C. (2011b). Small amplitude sharp pressure
687 waves to diagnose pipe systems. *Water Resources Management, 25*(1), 79-96.
688 doi:10.1007/s11269-010-9688-7
689 Meniconi, S., Brunone, B., Ferrante, M., & Massari, C. (2011c). Transient tests for locating and sizing
690 illegal branches in pipe systems. *Journal of Hydroinformatics, 13*(3), 334-345.
691 doi:10.2166/hydro.2011.012
692 Meniconi, S., Duan, H. F., Lee, P. J., Brunone, B., Ghidaoui, M. S., & Ferrante, M. (2013).
693 Experimental investigation of coupled frequency and time-domain transient test–based
694 techniques for partial blockage detection in pipelines. *Journal of Hydraulic Engineering, 139*(10), 1033-1040. doi:10.1061/(ASCE)HY.1943-7900.0000768
695
696 Munjal, M. L. (2014). *Acoustics of ducts and mufflers*: John Wiley & Sons.
697 Sattar, A. M., & Chaudhry, M. H. (2008). Leak detection in pipelines by frequency response method.
698 *Journal of Hydraulic Research, 46*(sup1), 138-151. doi:10.1080/00221686.2008.9521948
699 Sattar, A. M., Chaudhry, M. H., & Kassem, A. A. (2008). Partial blockage detection in pipelines by
700 frequency response method. *Journal of Hydraulic Engineering, 134*(1), 76-89.
701 doi:10.1061/(ASCE)0733-9429(2008)134:1(76)
702 Stephens, M. L. (2008). Transient response analysis for fault detection and pipeline wall condition
703 assessment in field water transmission and distribution pipelines and networks. (Ph.D. thesis),
704 Univ. of Adelaide, Adelaide, Australia.
705 Tuck, J., Lee, P. J., Davidson, M., & Ghidaoui, M. S. (2013). Analysis of transient signals in simple
706 pipeline systems with an extended blockage. *Journal of Hydraulic Research, 51*(6), 623-633.

707 doi:10.1080/00221686.2013.814599
708 Vardy, A. E., & Brown, J. M. B. (1995). Transient, turbulent, smooth pipe friction. *Journal of*
709 *Hydraulic Research, 33*(4), 435-456. doi:10.1080/00221689509498654
710 Wang, X., & Ghidaoui, M. S. (2018). Pipeline leak detection using the matched-field processing
711 method. *Journal of Hydraulic Engineering, 144*(6), 04018030.
712 doi:10.1061/(ASCE)HY.1943-7900.0001476
713 Wang, X. J., Lambert, M. F., & Simpson, A. R. (2005). Detection and location of a partial blockage in
714 a pipeline using damping of fluid transients. *Journal of Water Resources Planning and*
715 *Management, 131*(3), 244-249. doi:10.1061/(ASCE)0733-9496(2005)131:3(244)
716 Wylie, E. B., Streeter, V. L., & Suo, L. S. (1993). *Fluid transients in systems*. Englewood Cliffs, New
717 Jersey: Prentice-Hall.
718

719 **Figure Caption List**

720 **Fig. 1.** (a) Random and non-uniform blockages in real water pipelines (reprinted from Che et al.,
721 2018b, © ASCE); (b) sketch of a real pipeline with random and non-uniform blockages; (c) sketch of
722 a simplified pipeline with exponential non-uniform blockages used for analytical analysis.

723 **Fig. 2.** An unbounded pipeline system containing two symmetrical exponential non-uniform
724 blockages (with a wave generator and a wave receiver).

725 **Fig. 3.** Unbounded pipeline systems with (a) uniform blockages; (b) exponential non-uniform
726 blockages; and (c) linear non-uniform blockages.

727 **Fig. 4.** Energy transmission coefficients T_C of intact and blocked pipeline systems.

728 **Fig. 5.** (a) Measured pressure signals in the time domain ($\omega_c^* = 1$); (b) corresponding pressure signals
729 in the frequency domain ($\omega_c^* = 1$).

730 **Fig. 6.** Measured pressure signals in the time domain (a) $\omega_c^* = 0.5$, (c) $\omega_c^* = 1.5$, (e) $\omega_c^* = 2.5$;
731 corresponding pressure signals in the frequency domain (b) $\omega_c^* = 0.5$, (d) $\omega_c^* = 1.5$, (f) $\omega_c^* = 2.5$.

732 **Fig. 7.** Numerical validation of the derived energy transmission coefficient T_C.

733 **Fig. 8.** A bounded reservoir-pipeline-valve system.

734 **Fig. 9.** Transient frequency responses of bounded pipeline systems with both steady and unsteady
735 friction.

736 **Fig. 10.** Energy transmission coefficients T_C of bounded and unbounded pipeline systems.

737 **Fig. 11.** (a) Energy transmission coefficients T_C of unbounded non-uniform blocked pipeline systems;
738 (b) resonant frequency shifts of bounded systems induced by non-uniform blockages.

739 **Fig. 12.** (a) Energy transmission coefficients T_C of unbounded non-uniform blocked pipeline systems;
740 (b) resonant frequency shifts of bounded systems induced by non-uniform blockages.

741 **Fig. 13.** Sketches of the irregular blockage and its uniform and exponential non-uniform
742 approximations.
743 **Fig. 14.** The irregular blockage is approximated as (a) uniform blockage; (b) exponential non-uniform
744 blockages.
745

Tables

Table 1. Detailed pipeline system parameters for energy transmission coefficient T_C calculations

Blockage type	l_1 (m)	l_2 (m)	l_3 (m)	l_4 (m)	R (m)	$\|s\|$	R_C (m)
intact	300	100	100	500	0.25	0	0.25
uniform	300	100	100	500	0.25	0	0.2
exp non-uniform	300	100	100	500	0.25	4.64E-03	0.1572
linear non-uniform	300	100	100	500	0.25	1.00E-03	0.15

751

752

753 **Table 2.** Detailed system parameters for numerical validation

Blockage type	l_1 (m)	l_2 (m)	l_3 (m)	l_4 (m)	R (m)	$\|s\|$	R_C (m)	a_0 (m/s)
exp non-uniform	300	100	100	500	0.25	4.64E-03	0.1572	1000

754

755

756

757 **Table 3.** Detailed pipeline system parameters

Pipeline system	l_1 (m)	l_2 (m)	l_3 (m)	l_4 (m)	R (m)	R_C (m)	$\|s\|$	f
bounded	399	1	1	599	0.25	0.15	5.11E-01	0.02
unbounded	399	1	1	599	0.25	0.15	5.11E-01	0

758

759

760

761 **Table 4.** Detailed pipeline system parameters of bounded and unbounded pipeline systems

Test no.	l_1 (m)	l_2 (m)	l_3 (m)	l_4 (m)	R (m)	R_C (m)	$\|s\|$
T1	300	100	100	500	0.25	0.15	5.11E-03
T2	300	100	100	500	0.25	0.175	3.57E-03
T3	300	100	100	500	0.25	0.20	2.23E-03
T4	390	10	10	590	0.25	0.15	5.11E-02
T5	399	1	1	599	0.25	0.15	5.11E-01

762

763

764

765 **Table 5.** Settings of the experimental test system (Duan et al., 2017)

Blockage type	l_1 (m)	$l_b = l_2 + l_3$ (m)	l_4 (m)	R (mm)	a_0 (m/s)	$\bar{R}_b$ (mm)	$\bar{a}_b$ (m/s)
rough coir	15.58	5.54	20.41	36.6	1180	29.8	1010

766

Figures

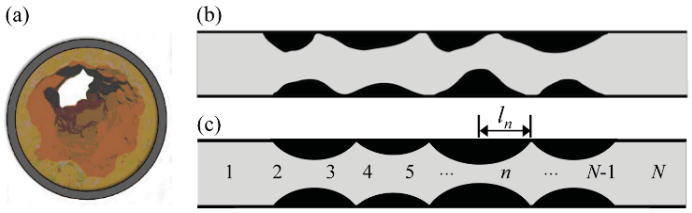

Fig. 1. (a) Random and non-uniform blockages in real water pipelines (reprinted from Che et al., 2018b, © ASCE); (b) sketch of a real pipeline with random and non-uniform blockages; (c) sketch of a simplified pipeline with exponential non-uniform blockages used for analytical analysis.

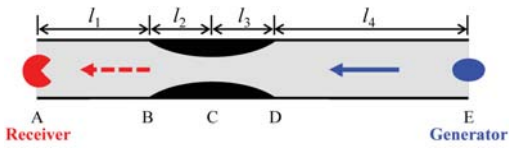

Fig. 2. An unbounded pipeline system containing two symmetrical exponential non-uniform blockages (with a wave generator and a wave receiver).

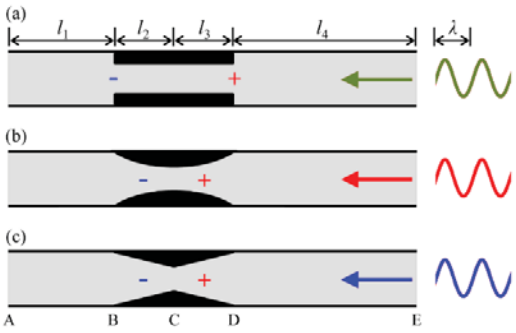

Fig. 3. Unbounded pipeline systems with (a) uniform blockages; (b) exponential non-uniform blockages; and (c) linear non-uniform blockages.

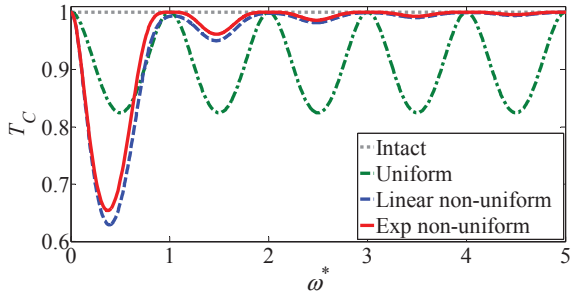

Fig. 4. Energy transmission coefficients T_C of intact and blocked pipeline systems.

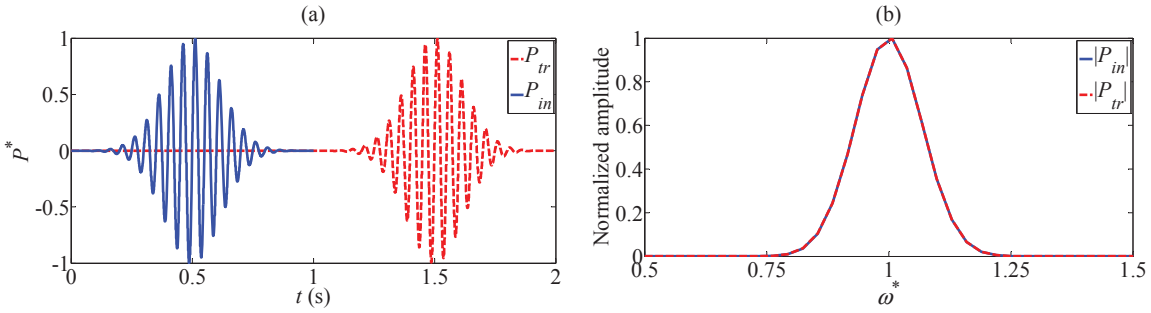

Fig. 5. (a) Measured pressure signals in the time domain ($\omega_c^* = 1$); (b) corresponding pressure signals in the frequency domain ($\omega_c^* = 1$).

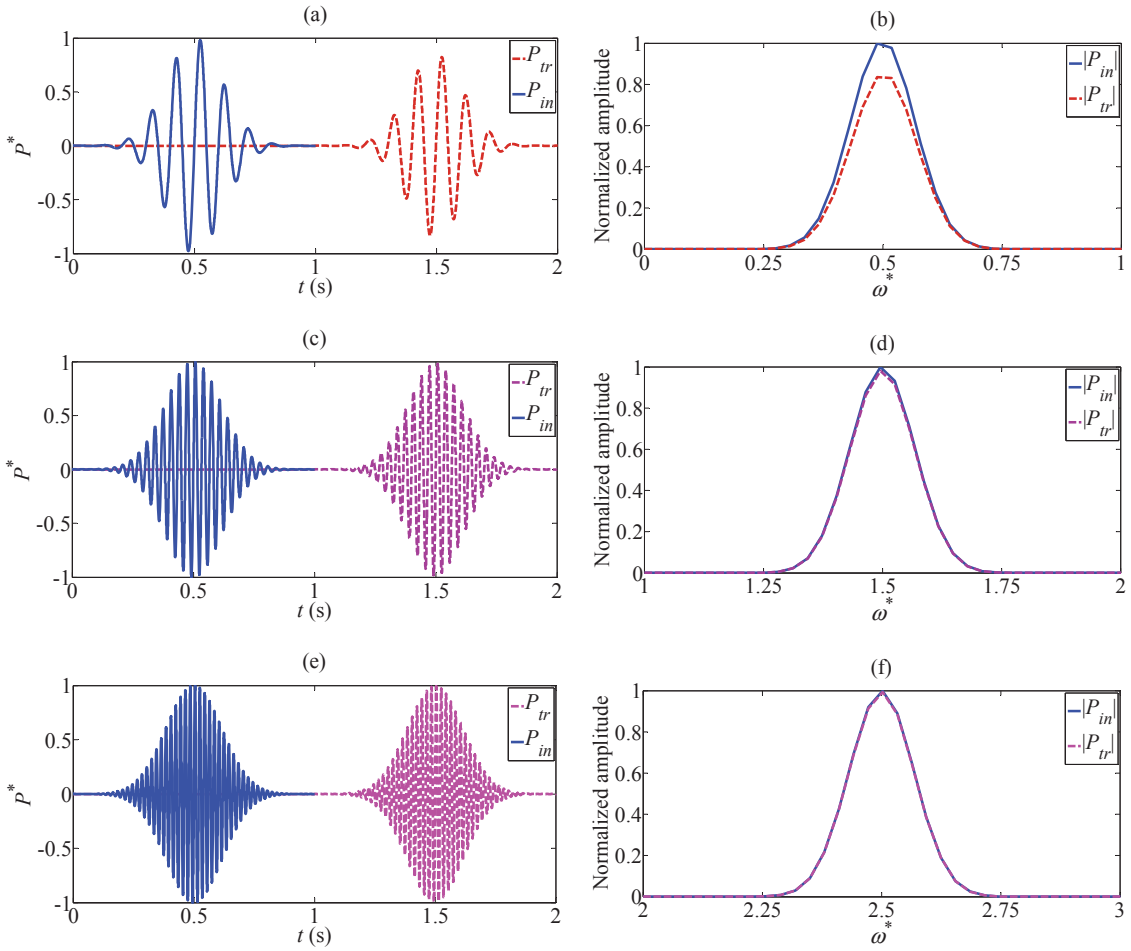

Fig. 6. Measured pressure signals in the time domain (a) $\omega_c^* = 0.5$, (c) $\omega_c^* = 1.5$, (e) $\omega_c^* = 2.5$; corresponding pressure signals in the frequency domain (b) $\omega_c^* = 0.5$, (d) $\omega_c^* = 1.5$, (f) $\omega_c^* = 2.5$.

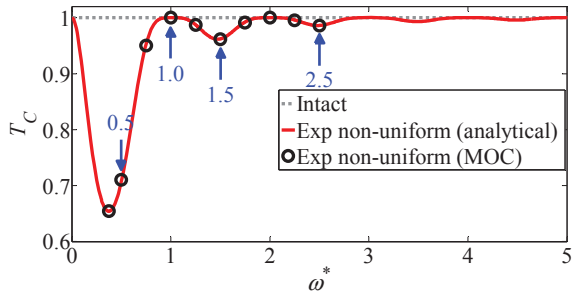

Fig. 7. Numerical validation of the derived energy transmission coefficient T_C.

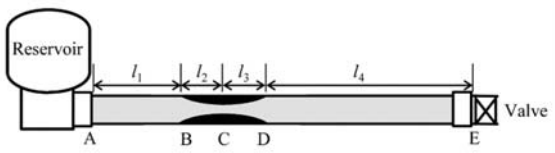

Fig. 8. A bounded reservoir-pipeline-valve system.

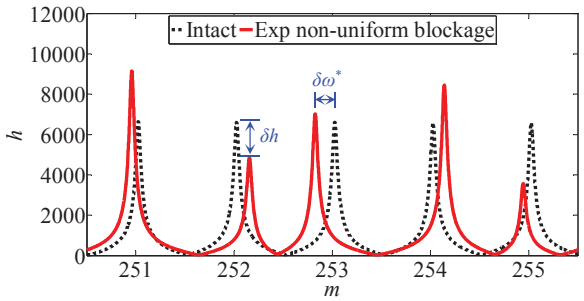

Fig. 9. Transient frequency responses of bounded pipeline systems with both steady and unsteady friction.

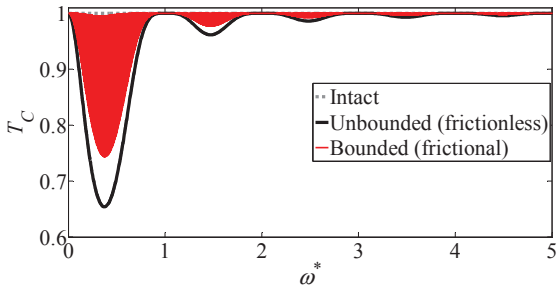

Fig. 10. Energy transmission coefficients T_C of bounded and unbounded pipeline systems.

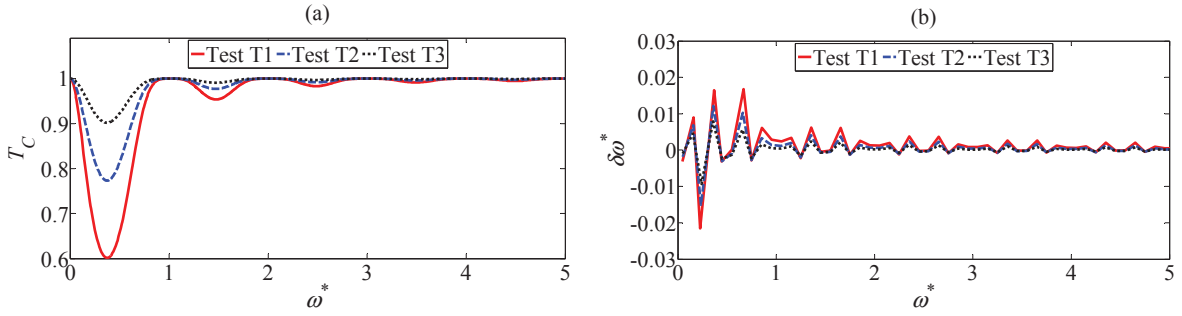

Fig. 11. (a) Energy transmission coefficients T_C of unbounded non-uniform blocked pipeline systems; (b) resonant frequency shifts of bounded systems induced by non-uniform blockages.

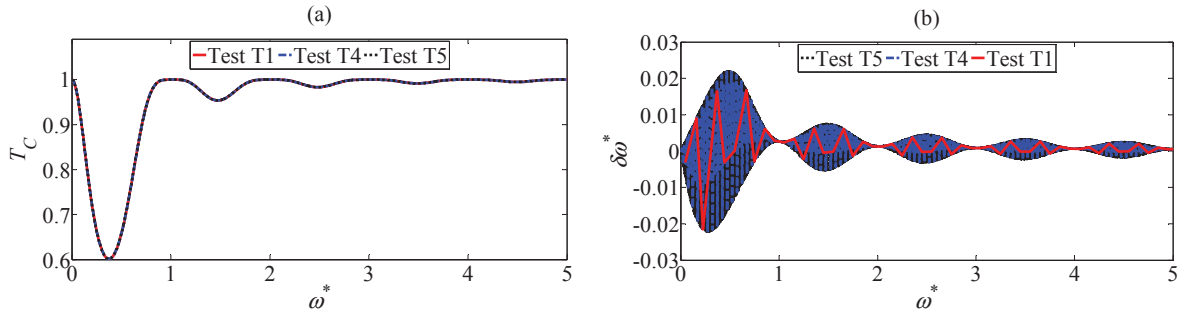

Fig. 12. (a) Energy transmission coefficients T_C of unbounded non-uniform blocked pipeline systems; (b) resonant frequency shifts of bounded systems induced by non-uniform blockages.

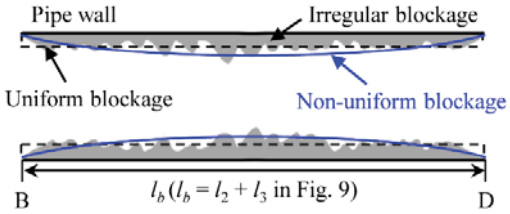

Fig. 13. Sketches of the irregular blockage and its uniform and exponential non-uniform approximations.

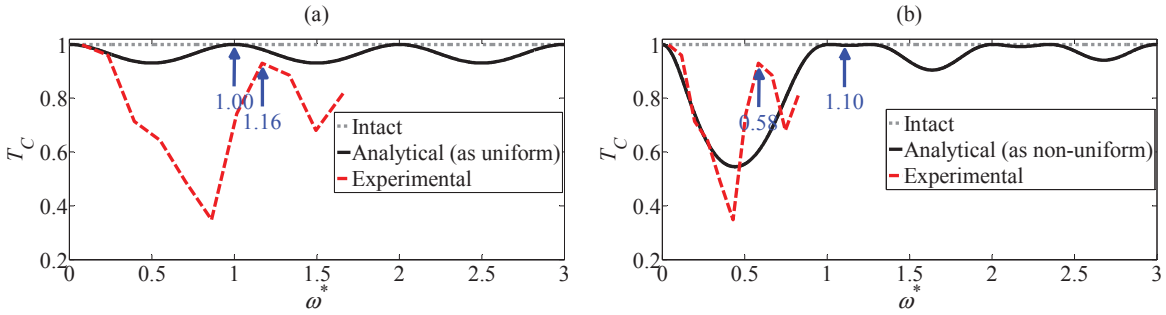

Fig. 14. The irregular blockage is approximated as (a) uniform blockage; (b) exponential non-uniform blockages.